Available online at www.sciencedirect.com
SCIENCE DIRECT
Thermochimica Acta 438 (2005) 41–50
thermochimica acta
www.elsevier.com/locate/tca

Kinetics of the thermal degradation of *Erica arborea* by DSC: Hybrid kinetic method

D. Cancellieri *, E. Leoni *, J.L. Rossi

SPE-CNRS UMR 6134, University of Corsica, Campus Grossetti, B.P. 52, 20250 Corti, France

Received 3 July 2005; received in revised form 22 July 2005; accepted 26 July 2005
Available online 9 September 2005

Abstract

The scope of this work was the determination of kinetic parameters of the thermal oxidative degradation of a Mediterranean scrub using a hybrid method developed at the laboratory. DSC and TGA were used in this study under air sweeping to record oxidative reactions. Two dominating and overlapped exothermic peaks were recorded in DSC and individualized using an experimental and numerical separation. This first stage allowed obtaining the enthalpy variation of each exothermic phenomenon. In a second time, a model free method was applied on each isolated curve to determine the apparent activation energies. A reactional kinetic scheme was proposed for the global exotherm composed of two independent and consecutive reactions. In fine mean values of enthalpy variation and apparent activation energy previously determined were injected in a model fitting method to obtain the reaction order and the preexponential factor of each oxidative reaction. We plan to use these data in a sub-model to be integrated in a wildland fire spread model.

Keywords: Wildland fire; Thermal degradation; Oxidation; Ligno-cellulosic fuels; Kinetics

1. Introduction

The effect of fire on Mediterranean ecosystems has been a research priority in ecological studies for several years. Nevertheless, in spite of considerable efforts in fire research, our ability to predict the impact of a fire is still limited, and this is partly due to the great variability of fire behaviour in different plant communities [1,2]. Flaming combustion of ligno-cellulosic fuels occurs when the volatile gaseous products from the thermal degradation ignite in the surrounding air. The heat released from combustion causes the ignition of adjacent unburned fuel. Therefore, the analysis of the thermal degradation of ligno-cellulosic fuels is decisive for wildland fire modelling and fuel hazard studies [3–5]. Physical fire spread models are based on a detailed description of physical and chemical mechanisms involved in fires. Since the pioneering work of Grishin et al. [6] these models incorporate chemical kinetics for the thermal degradation of fuels. However, kinetic models need to be improved.

Thermal degradation of ligno-cellulosic fuels can be considered according to Fig. 1.

We present hereafter the results obtained on *Erica arborea*, one of the most inflammable species in Mediterranean area. DSC curves showing two overlapped exothermic peaks (exotherms 1 and 2) were recorded at different heating rates under air. The fuel mass loss was recorded using TGA as an additional technique in order to get some information about the reactional mechanism. There are only a few DSC studies in the literature concerning the thermal decomposition of ligno-cellulosic materials which is preferably followed by TGA [7–9]. We adapted the DSC in order to measure the heat flow released by natural fuels undergoing thermal decomposition and in this paper we present a method to separate the thermal events from the global recorded exotherm. The two overlapped peaks observed on the DSC curves were experimentally and numerically isolated prior to the kinetic study.

The knowledge of the kinetic triplet (E_a, K_0 and n) and the kinetic scheme could help us in predicting the rate of thermal degradation when the collection of experimental is impossible in classical thermal analysis (high heating rates encountered in fire conditions). The thermal degradation kinetics of

* Corresponding authors. Tel.: +33 495 450 076; fax: +33 495 450 162.
E-mail addresses: cancelie@univ-corse.fr (D. Cancellieri), eleoni@univ-corse.fr (E. Leoni).

0040-6031/$ – see front matter © 2005 Elsevier B.V. All rights reserved.
doi:10.1016/j.tca.2005.07.013

Nomenclature

a_0, a_1, a_2, a_3	numerical parameters of the interpolation function
A	virgin fuel
B	evolved gases
B′	oxidation products
C	chars
D	ashes
E_a	activation energy (kJ/mol)
$f(\alpha)$	kinetic model reaction
ΔH	enthalpy of the reaction (endo up) (kJ/g)
I	interpolation function
KL	reaction rate of char and volatiles formation
K_0	preexponential factor (s^{-1})
K_1	reaction rate of reaction one
K_2	reaction rate of reaction two
Δm	variation of mass loss (%)
n	reaction order
r	correlation coefficient
R	gas constant 8.314 kJ/mol
RSS	residual sum of squares
t	time (min)
T	temperature (K)
x, y, z	interpolation coefficients

Subscripts

Cur	Curie point
deduct	deducted from experiment by subtraction
exo	exothermic
exp	experimental value
inter	interpolated
iso	experimentally isolated
melt	melting point
offset	end of phenomena
sim	simulated data
1	refers to exotherm 1
2	refers to exotherm 2

Greek symbols

α	conversion degree
β	heating rate (K/min)

Erica arborea was studied using a combination of two kinds of methods: free model methods and model fitting method. A free model method was applied in a first time to calculate the apparent activation energy and in a second time we used this result as initial data in a model fitting method to obtain preexponential factor, reaction order for our defined kinetic scheme. Our hybrid kinetic method is based on four stages (A–D) presented in this paper.

2. Experimental and methods of calculation

2.1. Experimental

Plant material was collected from a natural Mediterranean ecosystem situated far away from urban areas in order to prevent any pollution on the samples. *Cistus monspeliensis* (CM), *Erica arborea* (EA), *Arbutus unedo* (AU) and *Pinus pinaster* (PP) are representative species of the Corsican vegetation concerned by wildland fires. In the present work we chose to focus on the results obtained from EA samples. Naturally, the methodology developed hereafter is applicable to every ligno-cellulosic fuel.

Only small particles (<5 mm) are considered in fire spread [10]. Also, leaves and twigs were mixed, sampled and oven-dried for 24 h at 60 °C [11]. Dry samples were grounded and sieved to pass through a 1 mm mesh, then kept to the desiccator. The moisture content coming from self-rehydration was about 4% for all the samples.

We recorded the heat flow versus temperature (emitted or absorbed) thanks to a power compensated DSC (Perkin-Elmer®, Pyris® 1) and the mass loss versus temperature thanks to a TGA 6 (Perkin-Elmer®).

The DSC calibration was performed out using the melting point reference temperature and enthalpy reference of pure indium and zinc (T_{melt}(In) = 429.8 K, ΔH_{melt}(In) = 28.5 J/g, T_{melt}(Zn) = 692.8, ΔH_{melt}(Zn) = 107.5 J/g). Thermal degradation was investigated in the range 400–900 K under dry air or nitrogen with a gas flow of 20 mL/min. Samples around 5.0 ± 0.1 mg were placed in an open aluminium crucible and an empty crucible was used as a reference. The error caused by weighting gives an error of 1.9–3% on ΔH_{exp}.

We adapted the DSC for thermal degradation studies by adding an exhaust cover disposed on the measuring cell

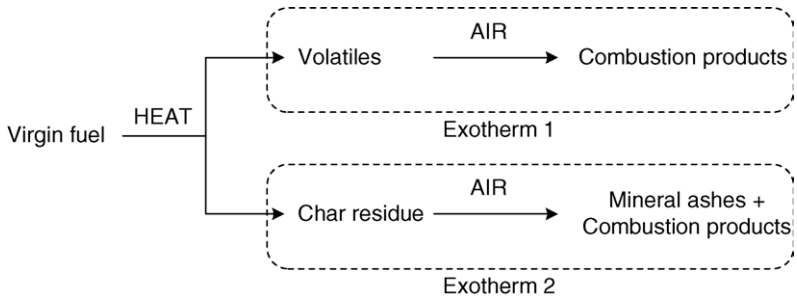

Fig. 1. Oxidative thermal decomposition of a ligno-cellulosic fuel.

(degradation gases escape and pressure do not increase in the furnaces). Several experiments were performed with different high heating rates (β = 10–40 K/min) in order to be closer to the wildland fires conditions. A significant variation between the heating rates ($\Delta\beta$ = 10 K/min) was very important for kinetics purpose.

The TGA calibration was performed using the Curie point of magnetic standards: Perkalloy® and alumel (T_{Cur}(alumel) = 427.4 K, T_{Cur}(Perkalloy®) = 669.2 K). Samples around 10.000 ± 0.005 mg were placed in an open platinum crucible and the degradation was monitored in the same range of temperature and heating rates as in DSC experiments.

2.2. Thermal separation

An experimental separation is very useful to indicate the way for a numerical treatment. Thanks to the switching of the surrounding atmosphere in the DSC furnaces we were able to define two independent and successive reactional schemes. The experimental conditions have been modified in order to hide the first exothermic phenomenon. Fig. 2 presents the schematic procedure we used to isolate the two phenomena with two experimental steps. The samples were thermally degraded under nitrogen atmosphere (step 1) at different heating rates from 400 to 900 K. Then the residual charcoal formed during the step 1 was used as a sample to be analyzed by DSC under air sweeping (step 2) with the same temperature range and heating rates as in step 1. Step 1 allowed to pyrolyze the fuels generating a char residue and volatiles which escaped in the surrounding non-oxidizing atmosphere.

2.3. Numerical separation

The mathematical interpolation performed with Mathematica® [12] gave equations describing the DSC curves. We fitted the global curve obtained under air with Eqs. (1) and (2). In a previous work [11] we used an empirical equation, with five adjustable parameters for each peak of each fuel, allowing the description of miscellaneous peaks and improved on temperature programmed desorption [13]. The following functions allowed a better fitting with only one parameters a_0 for Eq. (1) and three parameters a_1, a_2, a_3 for Eq. (2). These parameters were constant for all the species and heating rates. Mathematica® determined interpolation coefficient x, y and z in Eqs. (1) and (2). $T_{exo\,1}$, $T_{exo\,2}$ are the temperatures of exotherms 1 and 2, $T_{shoulder}$ is the temperature of a shoulder observed in exotherm 2 for all the species, $T_{exo\,1}$, $T_{exo\,2}$ and $T_{shoulder}$ were deducted using the derivative of the experimental plot.

The function which interpolates the set of experimental points is sought on the basis of Eq. (1) equation model [14] for exotherm 1:

$$I_1(T) = \sum_{i=1}^{5} x_i \exp(-a_0 i (T_{exo\,1} - T)^2) \tag{1}$$

and Eq. (2) equation model [14] for exotherm 2:

$$\begin{aligned} I_2(T) = {} & \sum_{i=1}^{5} y_i \exp(-a_1 i (T_{shoulder} - T)^2) \\ & + \sum_{i=1}^{15} z_i \left[1 + \exp\left(-\frac{T + a_2 \ln(ia_3) - T_{exo\,2}}{a_2}\right)\right]^{1-a_3} \\ & \times (ia_3)^{ia_3} (ia_3 + 1)^{(ia_3+1)} \\ & \times \exp\left(-\left(\frac{T + a_2 \ln(ia_3) - T_{exo\,2}}{a_2}\right)\right) \end{aligned} \tag{2}$$

with $a_0 = a_1 = 0.001$, $a_2 = 50$ and $a_3 = 0.04$ for all the experiments. We chose these functions because they are more robust than traditional function and avoids long compilation times. Values of parameters a_0, a_3 and n are arbitrary, a_1 is correlated to the peak top temperature and a_3 is correlated to the peak width.

In order to fit to a list of an experimental data, we use a Mathematica® function: "Fit[fun,data,var]". The data use have the form $\{\{T_1, I_1\},\{T_2, I_2\}, \ldots\}$. This function finds a least-squares fit to a list of this data as a linear combination of the functions "fun" of variable var(T). So, the solutions have

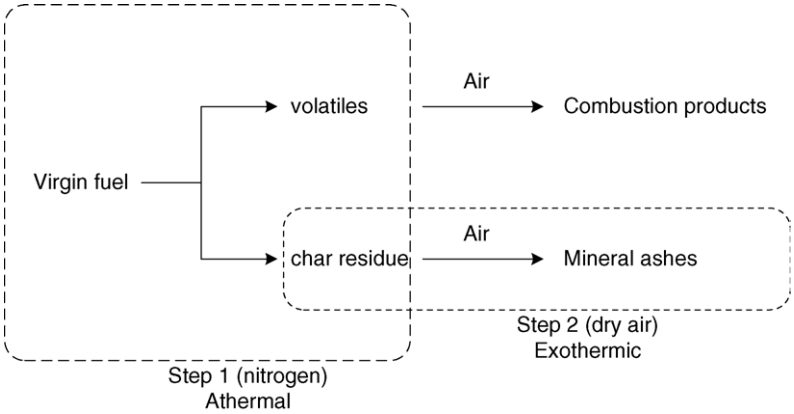

Fig. 2. Schematic representation of the experimental separation in two steps.

the form: $I(T)=C_0 + C_1\,\mathrm{fun} + C_2\,\mathrm{fun}^2 + \cdots + C_n\,\mathrm{fun}^n$ where the interpolation coefficients: $C_0, \ldots, C_n$ are given by Fit. In our case, Fit provides the solution: $C_i = x_i$ with $x_0 = 0$ for Eq. (1) and $C_i = \{y_i, z_i\}$ with $y_0 = z_0 = 0$ for Eq. (2).

In order to quantify the performance of the modelling procedure, for each experimental curve and the corresponding calculated one, Pearson's correlation (r) was measured and constrained to lie between −1 and 1. Variables are said to be negatively correlated, uncorrelated or positively correlated at temperature coordinates given by the experimental points.

2.4. Kinetic study

We have combined two kinds of kinetic methods: model free kinetics and model fitting kinetics.

Both are based on following equation:

$$\frac{\mathrm{d}\alpha}{\mathrm{d}t} = K_0 \exp\left(-\frac{E_\mathrm{a}}{RT}\right) f(\alpha) \tag{3}$$

Model free kinetics is based on an isoconversional method where the activation energy is a function of the conversion degree of a chemical reaction. For this work we chose the method of Kissinger–Akahira–Sunose (KAS) applied without any assumption concerning the kinetic model ($f(\alpha)$). The KAS method [15] simply consists of extending the Kissinger's method [16] to the conversion range 0.1–0.9, it is based on following equation:

$$\ln\left(\frac{\beta_i}{T_{jk}^2}\right) = \ln\left(\frac{K_{0\alpha}R}{E_{a\alpha}}\right) - \frac{E_{a\alpha}}{RT_{jk}} - \ln g(\alpha_k) \tag{4}$$

where $E_{a\alpha}$ and $K_{0\alpha}$ are, respectively, the apparent activation energy and the preexponential factor at a given conversion degree α_k and the temperatures T_{jk} are those which the conversion α_k is reached at a heating rate β_j. During a series of measurements the heating rate are $\beta = \beta_1 \cdots \beta_j \cdots$. The apparent activation energy was obtained from the slope of the linear plot of $\ln(\beta_i / T_{jk}^2)$ versus $1/T_{jk}$ performed thanks to a Microsoft® Excel® spreadsheet developed for this purpose. Four heating rates (10, 20, 30, 40 K/min) were used.

Model fitting kinetics is based on the fitting of Eq. (3) to the experimental values of $\mathrm{d}\alpha/\mathrm{d}t$. We used Fork® (CISP Ltd.) software which is provided for model fitting in isothermal or non-isothermal conditions. The resolution of ordinary differential equations was automatically performed by Fork® according to a powerful solver (Runge–Kutta order 4 or Livermore solver of ordinary differential equation). The reaction model $f(\alpha)$ was determined among six models specified in the literature [17]. Four heating rates (10, 20, 30, 40 K/min) were used at the same time; the software fit one kinetic triplet and one reaction model valid for all the heating rates. Once the determination of the best kinetic models and optimization of the parameters were achieved, the residual sum of squares between experimental and calculated values (RSS) indicated the acceptable "goodness of fit" from a statistical point of view. The results presented in Section 3 concern only the optimum parameters (best RSS value).

2.5. Hybrid kinetic method

Our hybrid kinetic method was built on four successive stages (A–B) from experimental data to simulated data. In stage A we individualized the exothermic phenomena. With stage B we obtained initiation data thanks to a model free method applied on each phenomenon. The model free results were used as an initialization of the model fitting method. In stage C we proposed a kinetic scheme with two oxidative reactions and a model fitting method gave the reaction model and the kinetic parameters of each phenomenon. Stage D was devoted to the simulation compared to experimental data in order to validate the method.

The application of our method to the thermal decomposition of *Erica arborea* gave the following results presented stage-by-stage in the next section.

3. Results and discussion

Fig. 3 shows the experimental DSC/TGA thermograms for an experiment performed at $\beta = 30$ K/min. In this section, figures present only plot obtained for one heating rate to but two exotherms are clearly visualized and associated with two mass loss for all the heating rates. We chose to present in this paper only the results obtained on *Erica arborea* fuel but the shape of thermograms from others fuels are very similar.

Table 1 presents the experimental results on the global exotherm in the range 400–900 K, values of enthalpy variation were obtained by numeric integration on the whole time domain and peak top temperatures were determined thanks to the values of the derivative experimental curve.

Table 2 presents the results from TGA measurement for the considered heating rates. The first mass loss is clearly higher (around 70%) than the second (around 27%). The maximum temperatures of mass loss were determined thanks to the derivative experimental plot.

During the first exothermic process the plant is pyrolyzed in the temperature range 400–600 K, contributing to the for-

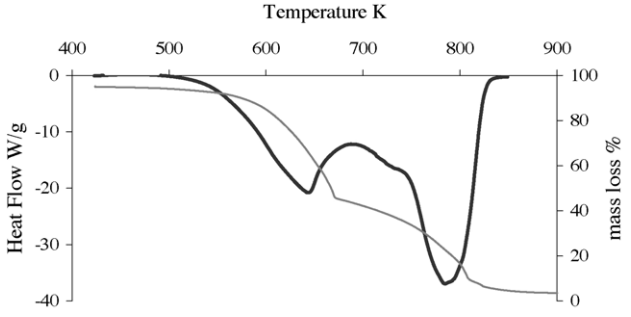

Fig. 3. DSC/TGA curves for EA fuel at 30 K/min under air sweeping.

Table 1
Peaks temperature at different heating rates for EA fuel by DSC.

β (K/min)	ΔH_{exp} [a] (kJ/g)	$T_{exo\,1}$ [b] (K)	$T_{exo\,2}$ [b] (K)
10	12.11	624	769
20	12.61	649	789
30	12.13	666	805
40	12.16	678	820

[a] Total enthalpy of combustion calculated by numerical integration of the experimental signal on the whole temperature range.
[b] $T_{exo\,1}$ and $T_{exo\,2}$ are the temperature of maximum value of heat flow obtained by DSC measurements.

Table 2
Offset temperature and mass lost at different heating rates for EA fuel by TGA

β (K/min)	Δm_1 (%)	$T_{offset\,1}$ [a] (K)	Δm_2 (%)	$T_{offset\,2}$ [a] (K)
10	68.3	644	27.4	796
20	69.4	660	28	808
30	77	676	26.6	819
40	66.2	693	28.6	832

[a] $T_{offset\,1}$ and $T_{offset\,2}$ are the temperature of maximum value of mass loss obtained by TGA measurements.

mation of char. Gases emission are visualized in TGA by a mass loss around 70%. An oxidation of these gases is possible when the surrounding atmosphere selected is air, this phenomenon is represented in DSC by the first exothermic peak. The second exothermic process can be considered like a burning process and it is known as glowing combustion. The char forms ashes in the temperature range of 600–900 K, TGA plots show a mass loss around 27% and the second exothermic peak is recorded in DSC. Other authors gave the same ascription for exotherms 1 and 2 [18–20].

We present hereafter the results obtained with the application of our original approach, the scope is the reduction a multi-step process in several independent steps.

3.1. Thermal and numerical separation: stage A

3.1.1. Thermal separation

As shown in Fig. 4, in the range 400–900 K, only the second exotherm is visualized in step 2 for all the species because only the remaining char was oxidized. Thus this experimental

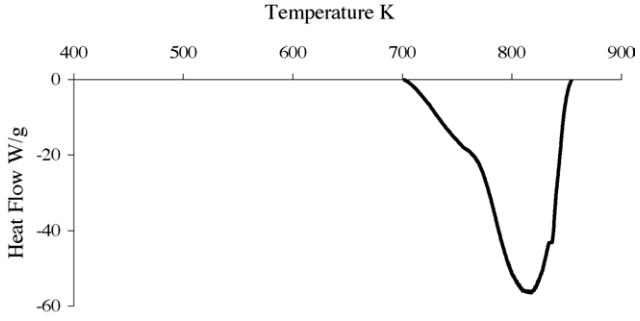

Fig. 4. DSC curve of residual char formed in step 1 at 30 K/min under air sweeping.

Table 3
Enthalpies variations of reaction 1 deducted and reaction 2 isolated

β (K/min)	$\Delta H_{1\,deduct}$ (kJ/g)	$\Delta H_{2\,iso}$ (kJ/g)
10	4.59	7.52
20	5.14	7.47
30	4.70	7.43
40	4.71	7.45

separation of exotherms 1 and 2 was very helpful to isolate the oxidation of char but the heat released by the oxidation of evolved gases could not been recorded.

We can deduct the variation of enthalpy for the first process by subtraction:

$$\Delta H_{1\,deduct} = \Delta H_{exp} - \Delta H_{2\,iso} \quad (5)$$

Table 4 shows the results of numeric integration of isolated curves for the second oxidation and the deduction of the enthalpy variation for the first one from Eq. (5).

The values of enthalpy variation are constant for each reaction of each plant. We were able to give a mean value for the enthalpy variation of the gases oxidation (exotherm 1) and for the oxidation of char (exotherm 2) for each species. The obtained values are close whatever the heating rate is.

3.1.2. Numerical separation

Thanks to the interpolation functions Eqs. (1) and (2) experimental DSC curves were reconstructed (exotherms 1 and 2) for all the heating rates considered.

Once the exotherms were plotted, enthalpy variation of each reaction was calculated by numerical integration of the signal and the results are shown in Table 4.

It is important to notice that the values obtained from the numerical treatment were found to be very close to those obtained by the thermal separation (cf. Tables 3 and 4). The thermal i.e. experimental separation can be considered as a validation of the numerical separation.

We can say that the energy released by the reaction referred to exotherm 2 is more important than the energy released by the reaction referred to exotherm 1. Actually, we found a mean value of 4.74 ± 0.14 kJ/g for the enthalpy variation of reaction referred to exotherm 1 with the associated mean value of mass loss of $70 \pm 7\%$ whereas we found a mean value of 7.45 ± 0.25 kJ/g for the enthalpy variation of reaction referred to exotherm 2 with an associated mean value of mass loss of $27 \pm 1\%$.

Fig. 5 is an example of experimental data compared to interpolated curves. For this experiment we obtained a value

Table 4
Enthalpies variations of reaction 1 interpolated and reaction 2 interpolated

β (K/min)	$\Delta H_{1\,inter}$ (kJ/g)	$\Delta H_{2\,inter}$ (kJ/g)
10	4.62	7.35
20	4.88	7.70
30	4.73	7.38
40	4.74	7.39

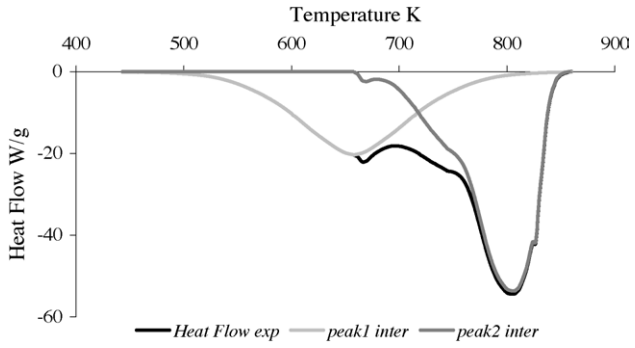

Fig. 5. Comparison between experimental and interpolated curves at 30 K/min.

of $r = 0.9946$. For all the species investigated and heating rates used the Pearson's correlation coefficient was about this value which indicates a very good fit. In the paper we present only results on experiments driven at $\beta = 30$ K/min in order to focus on the method we applied.

3.2. Initiation and prediction: stage B

In this stage, we used an isoconversional method in order to get initiation parameters (mean value of E_a) and also to have an idea of the mechanistic behaviour. Actually, the shapes of the dependence of E_a on α have been identified from simulated data for competing [21], independent [22], consecutive [23], reversible [24] reactions and as well as for reactions complicated by diffusion [25].

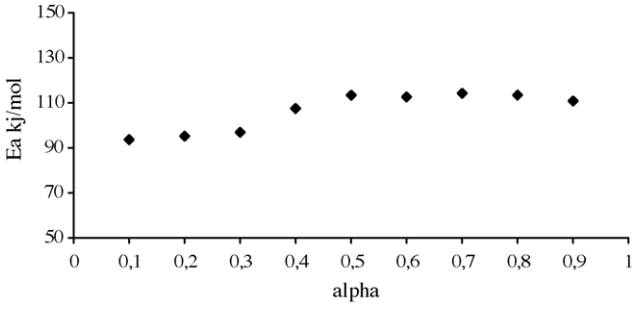

Fig. 6. KAS method for exotherm 1.

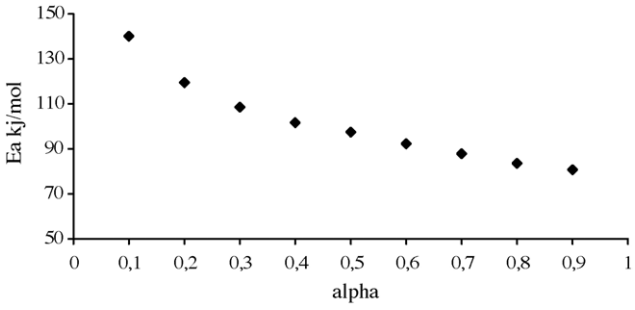

Fig. 7. KAS method for exotherm 2.

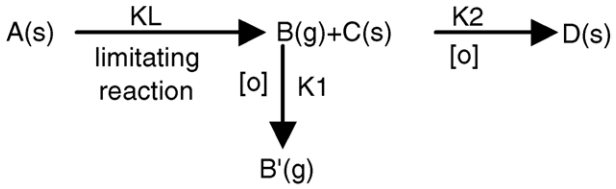

Fig. 8. Global reaction scheme.

Figs. 6 and 7 show the results of KAS method applied on exotherms 1 and 2. In the range 0.1–0.9, the global appearance of E_a confirms the fact that these two mechanisms are different.

Fig. 6 shows that the values of E_a increase from 90 to 110 kJ/mol in the range 0.1–0.4, while they are relatively constant (about 110 kJ/mol) in the range 0.4–0.9. We did not take into account this low variation and only the global shape of the dependence of E_a on α has been identified. Nevertheless, for the first process the E_a values are nearly constant ($\cong$100 kJ/mol) in the range 0.1–0.9. Thus, this exothermic reaction could be considered as a single step process.

For the totality of second process E_a values decrease from 140 to 90 kJ/mol with an exponential shape. This relatively important variation shows that the second exothermic process is probably a multi-step process. The convex shape visualized in Fig. 7 is indexed in the literature [26] like a typical oxidation in solid state. Such processes occur frequently in the degradation of charcoal that decomposes as chars → ashes + gas.

3.3. Modelisation: stage C

Let us consider the kinetics scheme represented on Fig. 8 and developed according to the results obtained in stages A and B.

We selected several reaction models [17] but the best results were obtained with a classical nth order reaction: $d\alpha/dt = K_0 \exp(-E_a/RT)(1-\alpha)^n$ for both exothermic processes and considering two independent reactions.

The first process is modelled as: $A_{(s)} \rightarrow C_{(s)} + B'_{(g)}$. The measured heat flow corresponds to the oxidation of evolved volatiles (exothermic) in gaseous state ($B_{(g)} \rightarrow B'_{(g)}$). Thus we studied indirectly the kinetics of $A_{(s)} \rightarrow C_{(s)} + B'_{(g)}$ by the kinetics of $B_{(g)} \rightarrow B'_{(g)}$ considering $A_{(s)} \rightarrow B_{(g)}$ as the rate limiting reaction of gas production. The second exothermic process concerns the oxidation of chars formed during the first process: $C_{(s)} \rightarrow D_{(s)} + E_{(g)}$.

The two processes can be traduced in the following differential equations considering a nth order model:

$$\frac{d\alpha_1}{dT} = \frac{1}{\beta} K_{01} \exp\left(-\frac{E_{a1}}{RT}\right)(1-\alpha_1)^{n_1} \quad (6)$$

$$\frac{d\alpha_2}{dT} = \frac{1}{\beta} K_{02} \exp\left(-\frac{E_{a2}}{RT}\right)(1-\alpha_2)^{n_2} \quad (7)$$

Table 5
Initiation data obtained in stages A and B

Initial data	
Exotherm 1	
$4.62 \leq \lvert\Delta H_1\rvert$ kJ/g ≤ 5.38	$80 \leq E_{a1}$ kJ/mol ≤ 120
Exotherm 2	
$7.35 \leq \lvert\Delta H_2\rvert$ kJ/g ≤ 8.20	$80 \leq E_{a2}$ kJ/mol ≤ 150

Table 6
Summary of kinetics results (model fitting) obtained for exotherms 1 and 2

Parameters	Results$_{1\,inter}$	Results$_{2\,inter}$
$\ln K_0$	13.2	12.9
E_a (kJ/mol)	95.3	116.3
n	1.68	0.49
$\lvert\Delta H\rvert$ (kJ/g)	4.98	7.56
r_{exo}	0.9972	0.9941

Data (mean values) obtained in previous stages A and B are taken as initiation entries for the model fitting method in Fork® software (cf. Table 5) for a conversion degree varying from 0.1 to 0.9.

The correlation coefficient and the RSS value helped us in identifying the "best" (statistically) set of parameters for a reaction model.

Table 6 presents the results obtained with the model fitting method, the parameters were calculated thanks to Fork® software and we present the best set of parameters for four heating rates (10, 20, 30 and 40 K/min). The first process of degradation has a coefficient of correlation $r_{exo\,1} = 0.9972$. In comparison the coefficient of correlation for the second process $r_{exo\,2}$=0.9941, although satisfactory, indicates a lower value than $r_{exo\,1}$, it means that the nth order model, would not correspond exactly to reality.

These results show that the mean values of E_a and ΔH determined in the previous stages were very close to the values presented in Table 6. To calculate the parameters with Fork® the previous stages were absolutely necessary in order to avoid erroneous values and strong compensation effects in the set of parameters and $f(\alpha)$.

The results testify the coherent choice of the model and the reaction pathway selected. An unsuited model would have generated a divergence in the parameter determination. Fork® software allowed us to verify the validity of initial data (E_a and ΔH) calculated previously since the calculated parameters of Table 6 were in the ranges defined in Table 5.

3.4. Simulation and prediction: stage D

In this stage we used a formal resolution of Eqs. (6) and (7) with Mathematica® software. The ordinary differential equation system was solved with the parameters calculated in stage C (Table 6). The resulting conversion degree was simulated on the whole temperature domain and allowed to plot the simulated heat flow. Figs. 9 and 10 show the comparison

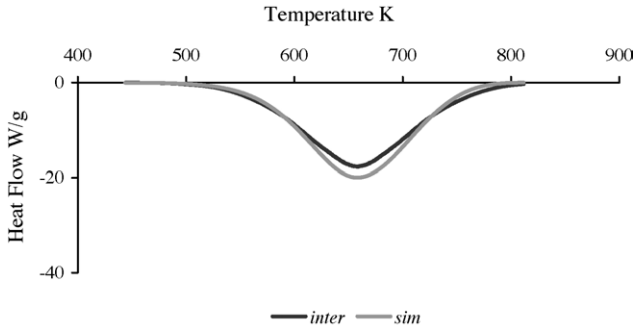

Fig. 9. Interpolated and fitted curves, exotherm 1 at 30 K/min, $r = 0.9972$.

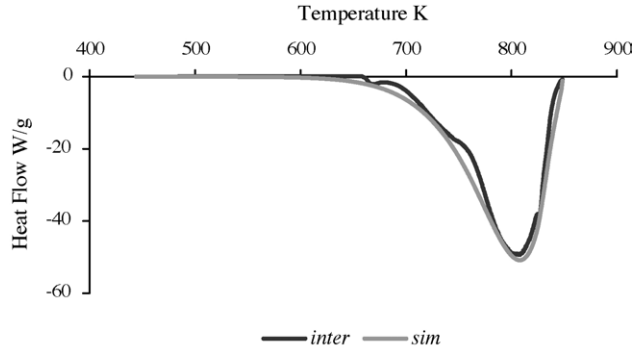

Fig. 10. Interpolated and fitted curves, exotherm 2 at 30 K/min, $r = 0.9941$.

between simulated plot and interpolated plot for exotherms 1 and 2. Fig. 11 shows the comparison between the total simulated plot (sum of Eqs. (6) and (7)) and the global experimental plot.

The correlation coefficient shows the good fit of the simulated data to experimental ones. Of course we only present here the results obtained at one heating rate but simulations have been performed at different heating rates with similar correlation coefficients. We tested the validity of calculated parameters and nth order models, simulations matched all our experimental data, we can simulate the thermal behaviour outside this range of temperature and heating rates, this will be presented in a future work.

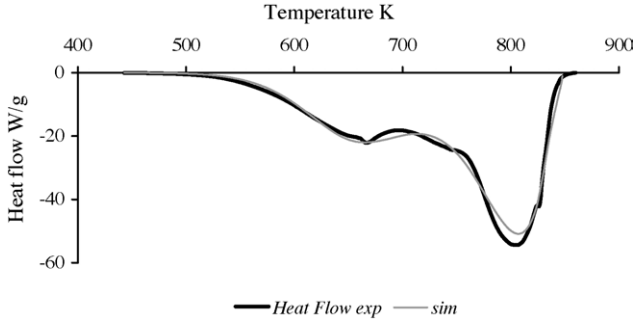

Fig. 11. EA fuel: experimental and fitted curves at 30 K/min, $r = 0.9924$.

4. Conclusion

As a general rule, reactions of thermal degradation show multi-step characteristics. They can involve several processes with different activation energies and mechanisms. On one hand, model free kinetics considering only one kinetic parameter, namely E_a is an over simplification of reality but they eliminate errors caused by an inappropriate kinetic model $f(\alpha)$. The validity of approaches, considering exclusively the activation energy values for the determination of the kinetics of solid-state reactions, can be hardly accepted [17]. On the other hand, even if model fitting methods give the kinetic triplet, they must be used carefully. Without an initiation step, results tend to produce highly ambiguous kinetic descriptions [17]. We have developed an original method combining the previous ones to study the kinetics of thermal degradation reactions. We applied this hybrid kinetic method to the thermal degradation of ligno-cellulosic fuels encountered in wildland fires. DSC experiments on such fuels showed two superposed exothermic phenomena. In a first step, we individualized (numerically and experimentally) these phenomena in two oxidative sub-reactions. Enthalpy variations of each sub-reaction were calculated. After this simplification the activation energies for exotherms 1 and 2 were determined using a model free method. Values of enthalpy variations and activation energies were used as initial data for the model fitting method. In this way only two parameters of the kinetic triplet have to be determinate. We proposed a kinetic scheme for the thermal degradation of ligno-cellulosic fuels under air with *n*th order model for the oxidative sub-reactions observed in DSC. Solid state kinetics computations should be carried out with experimental data obtained at several heating rates (not less than three) to ensure reliable results so, we performed this study with four heating rates (10, 20, 30, 40 K/min). The application of these techniques is widely recognized for the characterization of the degradation of solids [17]. Simulations obtained with the calculated parameters and considering two *n*th order reactions showed good fits to the experimental data. Such a method is promising to simulate heat flows at very high heating rates (outside the technical limits of classical TA).

In the field of wildland fires researches this approach could be useful since the step of thermal degradation of ligno-cellulosic fuels is still unknown. A sub-model of thermal degradation will be developed from this study and incorporated in a global physico-chemical fire spread model.

Acknowledgements

The authors express their gratitude to the autonomous region of Corsica for sponsoring the present work. This research was also supported by the European Economic Community. We are pleased to acknowledge V. Leroy for having actively participated to the experiments.

Appendix A

Figs. A1–A12 show the results of peak separation for experiments driven at 10, 20 and 40 K/min. One can also visualize the good fit of simulated data to experimental data for all the heating rates with the same set of parameters defined in Table 6.

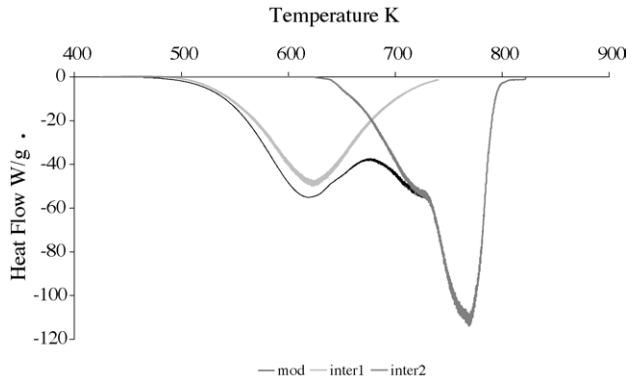

Fig. A1. Comparison between experimental and interpolated curves at 10 K/min.

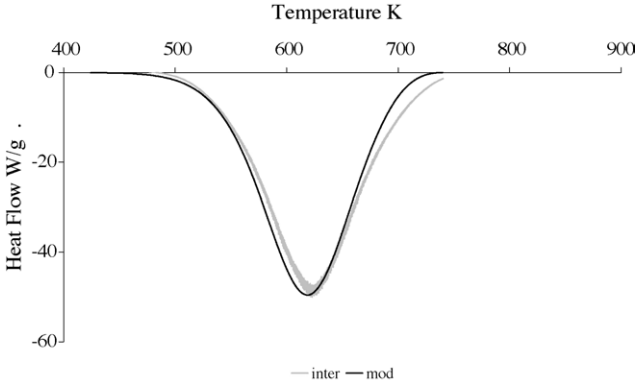

Fig. A2. Interpolated and fitted curves, exotherm 1 at 10 K/min.

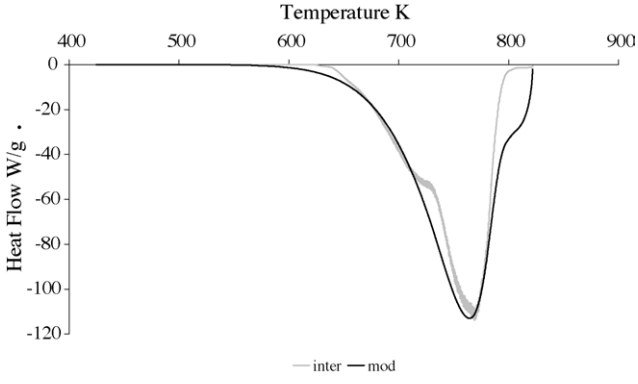

Fig. A3. Interpolated and fitted curves, exotherm 2 at 10 K/min.

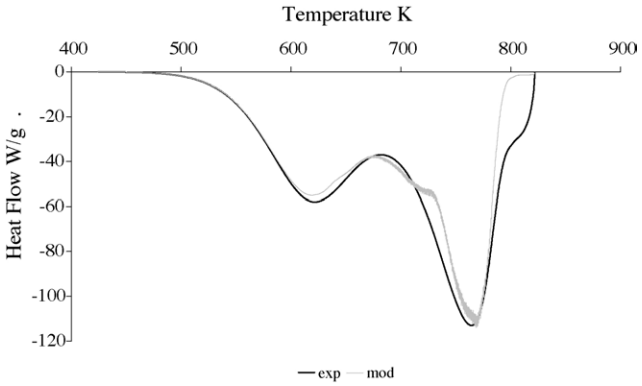

Fig. A4. EA fuel: experimental and fitted curves at 10 K/min.

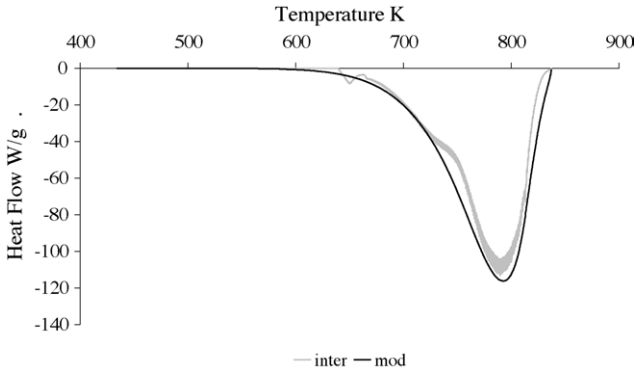

Fig. A7. Interpolated and fitted curves, exotherm 2 at 20 K/min.

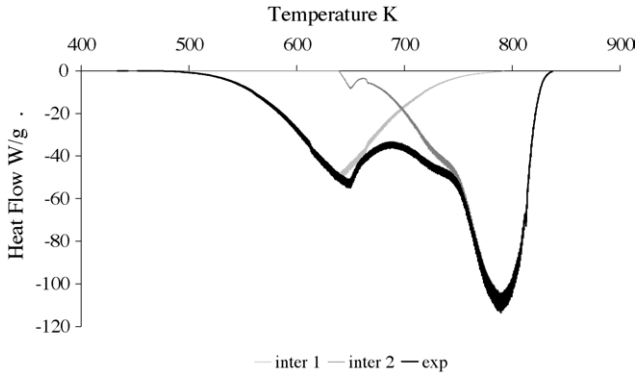

Fig. A5. Comparison between experimental and interpolated curves at 20 K/min.

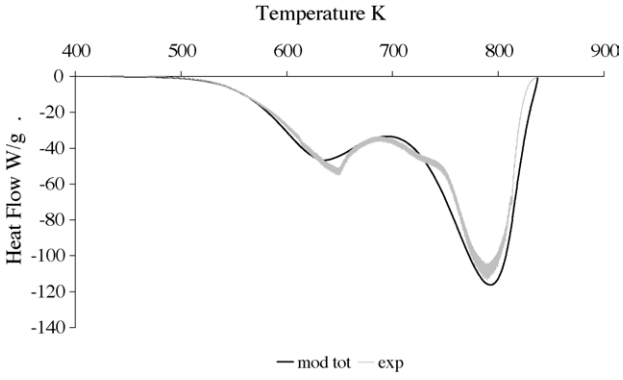

Fig. A8. EA fuel: experimental and fitted curves at 20 K/min.

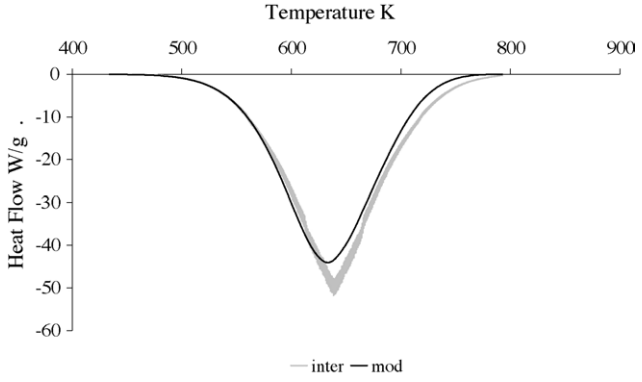

Fig. A6. Interpolated and fitted curves, exotherm 1 at 20 K/min.

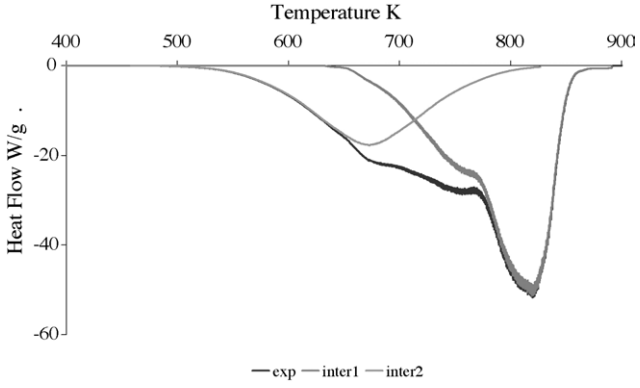

Fig. A9. Comparison between experimental and interpolated curves at 40 K/min.

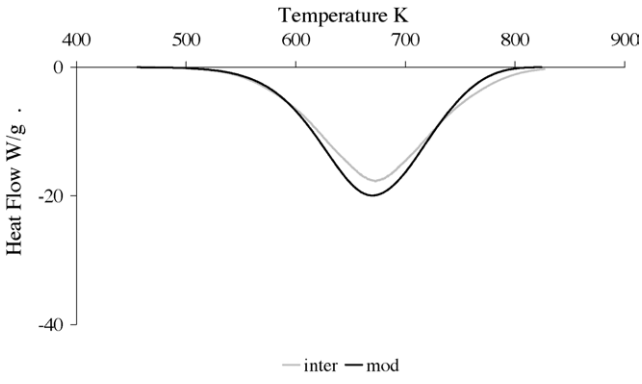

Fig. A10. Interpolated and fitted curves, exotherm 1 at 40 K/min.

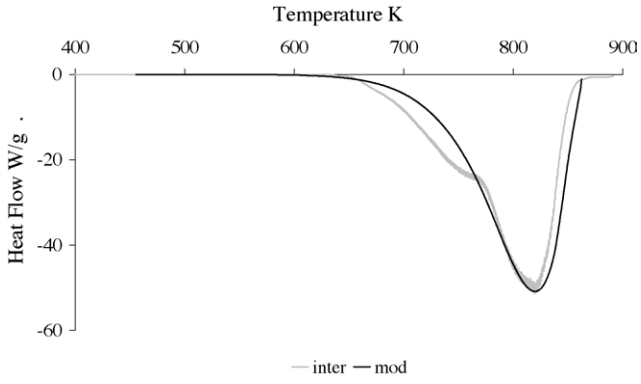

Fig. A11. Interpolated and fitted curves, exotherm 2 at 40 K/min.

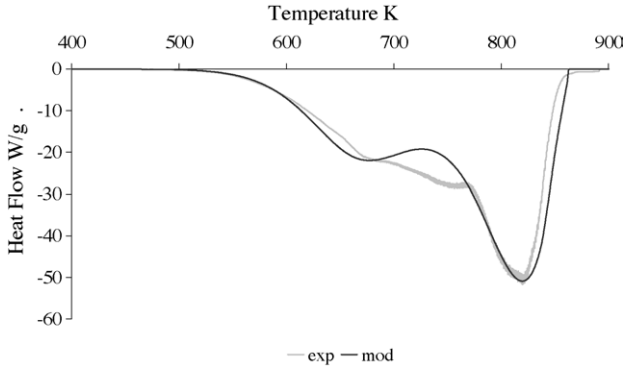

Fig. A12. EA fuel: experimental and fitted curves at 40 K/min.

References

[1] F.A. Albini, Combust. Sci. Technol. 42 (1985) 229.
[2] M. De Luis, M.J. Baeza, J. Raventos, Int. J. Wildland Fire 13 (2004) 79.
[3] A.P. Dimitrakopoulos, J. Anal. Appl. Pyrolysis 60 (2001) 123.
[4] R. Alèn, E. Kuoppala, P.J. Oesch, Anal. Appl. Pyrolysis 36 (1996) 137.
[5] J.H. Balbi, P.A. Santoni, J.L. Dupuy, Int. J. Wildland Fire 9 (2000) 275.
[6] A.M. Grishin, A.D. Gruzin, V.G. Zverev, Sov. Phys. Dokl. 28 (1983) 328.
[7] J. Kaloustian, A.M. Pauli, J. Pastor, J. Therm. Anal. 46 (1996) 1349.
[8] C.A. Koufopanos, G. Maschio, A. Lucchesi, Can. J. Chem. Eng. 67 (1989) 75.
[9] S. Liodakis, D. Barkirtzis, A.P. Dimitrakopoulos, Thermochim. Acta 390 (2002) 83.
[10] P. Caramelle, A. Clement, Research report, INRA, Avignon, 1978.
[11] E. Leoni, D. Cancellieri, N. Balbi, P. Tomi, A.F. Bernardini, J. Kaloustian, T. Marcelli, J. Fire Sci. 21 (2003) 117.
[12] T.B. Bahder, Mathematica for Scientists and Engineers, Addison-Wesley, Reading, 1995.
[13] R. Spinicci, Thermochim. Acta 296 (1997) 87.
[14] M. Abramowitz, I.A. Stegun, Handbook of Mathematical Functions, Dover, New York, 1965.
[15] T. Akahira, T. Sunose, Research report, vol. 16, CHIBA Institute of Technology, 1971, p. 22.
[16] H.E. Kissinger, Anal. Chem. 29 (1957) 1702.
[17] S. Vyazovkin, C.A. Wight, Int. Rev. Phys. Chem. 48 (1997) 125.
[18] J. Kaloustian, T.F. El-Moselhy, H. Portugal, Thermochim. Acta 401 (2003) 77.
[19] M.J. Safi, I.M. Mishra, B. Prasad, Thermochim. Acta 412 (2004) 155.
[20] C. Branca, C. Di Blasi, J. Anal. Appl. Pyrolysis 67 (2003) 207.
[21] S. Vyazovkin, A. Lesnikovich, Thermochim. Acta 165 (1990) 273.
[22] S. Vyazovkin, V. Goryachko, Thermochim. Acta 197 (1992) 41.
[23] S. Vyazovkin, Thermochim. Acta 236 (1994) 1.
[24] S. Vyazovkin, W. Linert, Int. J. Chem. Kinet. 27 (1995) 73.
[25] S. Vyazovkin, Thermochim. Acta 223 (1993) 201.
[26] S. Vyazovkin, C.A. Wight, Thermochim. Acta 340 (1999) 53.